Green Synthesis for MCM-41 and SBA-15 Silica Using the Waste Mother Liquor

Thianne Silva Batista Barbosa
Universidade Federal de Campina Grande
Thiago Rodrigo Barbosa Barros
Universidade Federal de Campina Grande
Tellys Lins Almeida Barbosa
Universidade Federal de Campina Grande
Meiry Gláucia Freire Rodrigues (meirygfr@hotmail.com)
Universidade Federal de Campina Grande https://orcid.org/0000-0003-2258-4230

Research Article

Keywords: MCM-41, synthesis, SBA-15, Mother liquor recycling, Green synthesis, Environmentally friendly

Posted Date: April 20th, 2021

DOI: https://doi.org/10.21203/rs.3.rs-411718/v1

Abstract

The synthesis of mesoporous materials such as MCM-41 and SBA-15 requires large amounts of water to neutralize the resulting products. The filtrate (mother liquor) therefore contains unreacted components that can be recycled and reused. The addition of the mother liquor in consecutive syntheses was carried out in order to evaluate the different effects on the physical and chemical properties of the mesoporous materials. For this purpose, the mother liquor from the initial synthesis (1st Generation) was saved and used for the second synthesis (2nd Generation) and successively for the third synthesis (3rd Generation). The three generations of each material were then characterized using different techniques such as X-ray diffraction, X-ray dispersive energy fluorescence, electron microscopy, infrared spectroscopy, Thermal behavior by thermogravimetric analysis and N_2 adsorption. The materials obtained showed similar diffractograms for the three generations and also showed similar percentages of silica through XRF. The SEM and IR results for molecular sieves showed the effectiveness of the processes of MCM-41 and SBA-15 synthesis using mother liquor. The results made it possible to observe that the structures of the materials had no significant differences in their physical and chemical properties, favoring the use of mother liquor for up to three generations.

1 Introduction

Mesoporous materials are a class of solids that have uniform pore sizes (1.5 to 40 nm), large surface areas (up to 2500 m^2.g-1), large pore volumes, excellent thermal stability, and structures that can be modified in different ways [1]. These materials are of great interest, mainly as catalysts [2] and adsorbents [3]. The mesostructured molecular sieves in the 2D group (MCM-41 and SBA-15) have hexagonal symmetry and are easier to produce than those of other groups [4]. Several models have been proposed to explain the formation of mesoporous materials that provide a rational basis for the various synthesis routes. In general, these models are based on the presence of surfactants in a solution that guide the formation of the inorganic mesostructure [5, 6].

The typical synthesis process for MCM-41 involves reagents such as: the silicon source, which serves to build the structure of the walls of the mesoporous material, the most commonly-used being pyrolyzed silica (Aerosil), tetraethyl orthosilicate (TEOS), and sodium silicate; surfactants, which are molecules with hydrophilic and hydrophobic characteristics that serve to guide the formation of the mesoporous structure, with cetyltrimethylammonium (CTABr) in chloride, bromide, or hydroxide form being the most commonly-used [7]; the hydroxyl source, which provide the organic cation that assists in the formation of basic silica construction units, with the most commonly-used being tetramethylammonium hydroxide (TMAOH) and ammonium hydroxide (NH_4OH) [8].

The SBA-15 molecular sieve is synthesized in an acidic medium with the use of cationic surfactants, a nonionic oligomeric or triblock copolymer, and directing agent for highly-ordered porous crystal structures. Conventional synthesis of SBA-15 is also performed using tetraethylorthosilicate (TEOS), tetramethylorthosilicate (TMOS), or sodium silicate as a silica source [9].

During the synthesis of these materials, the desired solid crystals are separated from the reaction mixture and the filtrate (mother liquor), which is rich in organic and inorganic species, is often unusable [10, 11]. The direct disposal of the mother liquor will not only lead to the waste of raw materials, but can also cause environmental pollution [12]. Some authors address the reuse and recycling of mother liquor as a raw material for the syntheses of porous materials [13–18]. To make synthesis processes more attractive, the principles of green chemistry have been implemented as concepts and actions related to economy, sustainability of resources, and environmental protection [19]. The Twelve Principles of Green Chemistry are "rules" that help chemists achieve the goal of sustainability and are characterized by careful planning of chemical synthesis processes in order to reduce adverse consequences [20].

This study is part of a line of research developed at the Laboratory for the Development of New Materials-LABNOV at UFCG. This line of research covered a series of studies on the synthesis and characterization of molecular sieves through different processes [21–35]. This study aims to reuse the mother liquor in three subsequent syntheses of the SBA-15 and MCM-41 molecular sieves to assess any possible changes in the physical, chemical, and morphological properties of each material.

2 Materials And Methods

2.1 Materials

Poly(ethylene glycol)block-poly(propylene glycol)block-poly(ethylene glycol) copolymer (Pluronic P123, PEG, 30%), cetyltrimethylammonium bromide (CTAB, 98%), hydrochloric acid (HCl, 37%), ammonium hydroxide (NH_4OH, 29%) and tetraethylorthosilicate (TEOS, 98%) were purchased from SIGMA-ALDRICH (MERCK).

2.2 Synthesis of molecular sieves MCM-41 and SBA – 15 using mother liquor

The MCM-41 1G molecular sieve was conventionally synthesized using the hydrothermal method, according to the procedure described by [8]. This synthesis consisted of dissolving the CTAB (structure-directing agent) in deionized water at 50°C under agitation for 30 min. The solution was cooled to approximately 25°C and NH_4OH was added under stirring at room temperature for 15 min. Then, the TEOS silica source was slowly added to the reaction medium and kept under stirring for 2 h. The gel obtained was placed in autoclaves and heated in an oven at 30°C for 24 h.

The conventional synthesis of the SBA-15 1G molecular sieve was based on the methodology described by [9]. The Pluronic P123 surfactant was dissolved in concentrated HCl and water, under stirring and heated at 35 ºC for 4 h. Following this, TEOS was added and the synthesis was aged under agitation and heated at 35 ºC for 24 hours. The material was then taken to the oven for hydrothermal treatment at 100°C for 48 h in a teflon crucible wrapped in a stainless-steel autoclave.

After crystallization, the as-prepared materials were separated by filtration into raw MCM-41 or SBA-15 and mother liquor. Molecular sieves were dried in an oven at 60°C for 24 h, after which they were subjected to the calcination process in a muffle furnace at 550°C for 7 h with a heating ramp of 5°C.min^{-1} to remove the organic template.

The syntheses of the materials in consecutive generations (MCM-41 2G; MCM-41 3G; SBA-15 2G; and SBA-15 3G) occurred similarly to the procedures already described. However, the mother liquor (ML) collected in traditional hydrothermal synthesis of molecular sieves (MCM-41 1G or SBA-15 1G) was added during the initial stage of the synthesis without modifications, replacing the mass corresponding to the water needed to form the reaction mixture. The reaction mixtures and the molar composition of each material can be seen in Table 1.

Table 1
Molar composition used in the synthesis of each material.

Material	Molar Composition
MCM-41 1G	*1 SiO_2: 0,3 CTABr: 11 NH_3: 144 H_2O*
MCM-41 2G	*1 SiO_2: 0,3 CTABr: 11 NH_3: 144 LM-I*
MCM-41 3G	*1 SiO_2: 0,3 CTABr: 11 NH_3: 144 LM-II*
SBA-15 1G	*1,0 SiO_2: 0,017 P_{123}: 5,7 HCl: 193 H_2O.*
SBA-15 2G	*1,0 SiO_2: 0,017 P_{123}: 5,7 HCl: 193 LM-I.*
SBA-15 3G	*1,0 SiO_2: 0,017 P_{123}: 5,7 HCl: 193 LM-II.*

2.3 Characterizations

For the characterization of the synthesized and calcined samples by XRD (X-ray diffraction), a Shimadzu XRD-6000 diffractometer was used, with CuKα radiation, a voltage of 40 KV, a current of 30 mA, a step size of 0.020 and a time per step of 0.60 seconds, with a sweep speed of 2º per minute and 2θ angle ranging from 1° to 10°. To obtain the infrared, IR VERTEX 70 equipment from BRUKER was used. The samples in the form of tablets were dried in an oven in advance and placed in the sample holder. The IR spectra were obtained at wavelengths in the 400–4000 cm^{-1} range with a resolution of 4 cm^{-1}. To identify and quantify the chemical composition of the synthesized samples, an S2 Ranger Bruker dispersive energy X-ray spectrophotometer was used. To perform microscopy on the samples. a VEGAS TESCAN scanning electron microscope was used. The powder samples were covered with a thin layer of gold by a metallizer and fixed to a support with carbon adhesive tape. Thermogravimetric analysis was performed in a Shimadzu DTG-60H Thermal Analyzer in a nitrogen atmosphere with a gas flow of 100 mL.min^{-1}.

3 Results And Discussion

3. 1 Characterization of raw materials

Figure 1 (a) shows the diffractograms of the samples of MCM-41 synthesized initially (MCM-41 1G) and from the following generations MCM-41 2G and MCM-41 3G. The diffractograms of the synthesized SBA-15 samples (SBA-15 1G, SBA-15 2G and SBA-15 3G) are shown in Fig. 1 (b).

According to [7, 8], the X-ray diffractograms in Fig. 1 (a) show that the materials obtained are characteristic of the MCM-41 molecular sieve in all three generations. The XRD's of the synthesized MCM-41 molecular sieves show an intense peak at 2θ = 2.2°, corresponding to the (1 0 0) plane and two to three smaller peaks between 3.5° and 6.0° due to the (1 1 0), (2 0 0), and (2 1 0) planes, indicating the presence of ordered mesoporous hexagonal MCM-41 [19, 36, 37]. A decrease in intensity for the first peak and the disappearance of the last peak for the samples MCM-41 2G and MCM-41 3G in relation to MCM-41 1G can be observed. Due to the substances present in the mother liquor, this decrease in pore ordering can be attributed to the pH variation that occurs when it is added to the reaction mixture [18].

According to what was described by [9], the diffractograms in Fig. 1 (b) show that the synthesized materials are characteristic of the SBA-15 molecular sieve. Note the presence of three well-defined peaks in all generations, which indicates a good uniformity of materials. The presence of the first reflection peak of the (1 0 0) plane at 2θ = 0.9° and of the (1 1 0) and (2 0 0) planes at 2θ = 1.6° and 1.8°, respectively, preserve the characteristic patterns of the SBA-15 mesostructure with reflections associated with a p6mm hexagonal symmetry of the mesoporous material [9, 27, 28, 31, 32, 38, 39].

Chemical analyses of all generations of MCM-41 obtained through ED-XRF showed a high content of silicon dioxide SiO_2 (94.37 %, 95.36 %, and 92.98 % in the first, second, and third generations, respectively) in the compositions as reported by [40] and some impurities such as aluminum trioxide (Al_2O_3) and metal Bromo (Br) from of the surfactant salt, CTAB. Chemical analyses determined through ED-XRF of the synthesized SBA-15 samples (SBA-15 1G, SBA-15 2G, and SBA-15 3G) indicate that SBA-15 is composed essentially of SiO_2 (100.00 %, 99.97 %, and 99.99 % in the first, second and third generations, respectively). These samples appeared to be chemically pure because they did not present impurities. Samples of the SBA-15 molecular sieve consisting only of Si and O were observed in the study by [41].

The spectra of the synthesized (MCM-41 1G, MCM-41 2G, and MCM-41 3G) and calcined (MCM-41 1G Cal, MCM-41 2G Cal, and MCM-41 3G Cal) samples are shown in Fig. 2 (a) and (b), respectively. The spectra of the synthesized (SBA-15 1G, SBA-15 2G, and SBA-15 3G) and calcined (SBA-15 1G Cal, SBA-15 2G Cal, and SBA-15 3G Cal) samples are shown in the Fig. 2 (c) and (d), respectively.

The spectra of the synthesized and calcined MCM-41 samples from all generations, presented in Fig. 2 (a), (b), (c), and (d), show bands in the 500–4000 cm^{-1} region that are characteristic of the fundamental vibrations of the functional groups present in the structures of molecular sieves MCM-41 and SBA-15 [42]. In Fig. 2 (a) and (b), the spectra have bands between 920 and 950 cm^{-1} corresponding to the

angular vibrations of the Si-OH bond of the silanol groups existing in the MCM-41 structure. In the 1000–1250 cm^{-1} region, it is possible to observe the presence of a broad band composed of two other bands, a main band at 1050 and 1066 cm^{-1} and a less-developed secondary band at 1025 and 1190 cm^{-1}. These correspond to asymmetric stretching of the Si-O-Si bond [18, 42]. In the spectra of the non-calcined samples, the vibrational bands at 1465 cm^{-1} and 2920 cm^{-1} are attributed to stretching between the CH of the CH_2 and CH_3 groups that correspond to the presence of the salt CTAB, which is occluded in the MCM-41 pores [43, 44].

The spectra of the synthesized and calcined SBA-15 samples presented in Fig. 2 (c) and (d) show a band around 787–850 cm^{-1} that corresponds to the symmetrical stretching of the Si-O-Si bond, very common in MCM-41 and SBA-15 type materials [43]. Another band at 930–1010 cm^{-1} corresponds to the angular vibration of the Si-OH bond of the silanol groups in the SBA-15 structure. In the 1065–1270 cm^{-1} region, it is possible to observe the presence of wide bands at 1065, 1070, and 1150 cm^{-1} and other less-developed bands at 1220, 1270 and 1205 cm^{-1}, in the first, second, and third generation samples, respectively. In the calcined samples, the main bands are at 1060, 1050, and 1060 cm^{-1} and the secondary bands are at 1211, 1211, and 1203 cm^{-1}, in the first, second, and third generation samples, respectively. These values all correspond to asymmetric stretching of the Si-O-Si bond [45]. In the spectra of the non-calcined samples, the vibrational bands at around 2890, 2969, and 2885 cm^{-1} refer to the vibrations of the organic molecule of the Pluronic P123 structural driver due to the stretching in the CH bonds of the CH_2 and CH_3 groups [46, 47]. After calcination, these bands disappear, indicating the removal of the surfactant from the material structure [48].

Figure 3 shows the images obtained through SEM for the synthesized MCM-41 samples (MCM-41 1G, MCM-41 2G, and MCM-41 3G) and synthesized SBA-15 samples (SBA-15 1G, SBA-15 2G, and SBA-15 3G).

The morphologies presented by the MCM-41 and SBA-15 molecular sieves can be diverse and are directly dependent on the synthesis conditions, such as: agitation, pH, aging temperature, hydrothermal synthesis temperature, aging time, and hydrothermal synthesis time, among others [49]. According to Fig. 3, the micrographs obtained through SEM of the synthesized MCM-41 samples show a morphology similar to those found by [50] who synthesized MCM-41 using NH_4OH at different temperatures. The particles have irregular and non-uniform spherical clusters in all generations [51]. In Fig. 3, the SBA-15 micrographs show nanochannels that are well-ordered and aligned with the direction of the fibers for samples from the three generations. They present similar morphologies to those found by [5, 52], with micrometric silica fibers formed from the linear adhesion of nodules of sub-micrometric particles, giving the appearance of interlaced bead necklaces [53].

Figure 4 shows the adsorption and desorption isotherms of the MCM-41 and SBA-15 samples, obtained through the BET method. All samples exhibited type IV isotherms, according to the IUPAC classification, with different hysteresis loops shown for the MCM-41 and SBA-15 samples [54].

According to IUPAC, isotherms of the type shown in Fig. 4 are typical of mesoporous materials with multilayer adsorption cycles. Initially, nitrogen adsorption occurs on the material surface at a relative pressure (P/P_0) below 0.2. After the monolayer is formed, multi-layers develop over it. From a (P/P_0) of 0.4 there is an increase in the capacity of adsorbed nitrogen, called hysteresis, associated with capillary nitrogen condensation in the mesopores [37]. This behavior is observed for all generations of the samples. In the final part of the isotherm, after capillary condensation, the pore is saturated and a small amount of N_2 is adsorbed on the outer walls, resulting in a maximum volume of adsorbed gas of approximately 450, 430, and 410 $cm^3.g^{-1}$ for MCM-41 1G, 2G, and 3G, respectively. For SBA-15 these values are 500, 540, and 595 $cm^3.g^{-1}$ in the first, second, and third generations, respectively. The isotherm for the MCM-41 sample exhibited H4 type hysteresis, corresponding to porous materials made up of narrow, slit-shaped pores. For SBA-15, the isotherm showed hysteresis of type H1 [23, 51] associated with porous materials that consist of agglomerates or compact groups of uniform spheres in a regular arrangement and, therefore, have narrow pore size distributions.

The graphs of the pore distributions of the MCM-41 and SBA-15 samples, as obtained through the BJH method, are shown in Fig. 5 (a) and (b), respectively.

The pore diameter distribution in Fig. 5 (a) showed peaks between 2 and 3 nm for the three generations of MCM-41, which are attributed to the microporous region, and also a peak at 36 nm in the first generation only, which is attributed to the mesoporous region. For SBA-15, the pore distribution graph in Fig. 5 (b) showed all peaks of the three sample generations to be between 6 and 7 nm, all attributed to the micropore region.

According to Table 2, the BET surface area of MCM-41 1G was 726 $m^2.g^{-1}$ and for the following generations this value increased to 818 and 867 $m^2.g^{-1}$ for MCM-41 2G and MCM-41 3G, respectively. For the pore wall thickness of the MCM-41structures, a similar behavior can be seen, in which the values increased in the following generations, to 2 and 2.22 in the second and third generations, respectively. These values are higher than those found in the literature [5], which indicates standard values of Wt (nm) for MCM-41 between 1 and 1.5 nm.

Table 2
Synthesis parameters and characterization of the samples

	a_0 (nm)	S_{BET} ($m^2.g^{-1}$)	Dp BJH (nm)	Vp ($cm^3.g^{-1}$)	Wt (nm)
MCM-41 1G	4.87	726	3.53	0.64	1.34
MCM-41 2G	5.07	818	3.07	0.62	2.00
MCM-41 3G	5.02	867	2.80	0.63	2.22
SBA-15 1G	11.59	550	5.53	0.77	6.06
SBA-15 2G	11.92	561	5.92	0.83	6.00
SBA-15 3G	11.59	600	6.08	0.91	5.51

Table 2 shows the values obtained for the network parameter, a_0 (nm), which can be calculated in a simplified manner, $a_0 = 2d_{100}.(31/2)-1$, where d100 corresponds to the interplanar distance of the (1 0 0) diffraction plane; the surface area, S_{BET} ($m^2.g^{-1}$), obtained by the BET method; and the average pore diameter, Dp (nm), obtained by the BJH method. Vp ($cm^3.g^{-1}$) corresponds to the pore volume of the samples and W_t corresponds to the nanometer thickness of the structural wall, calculated as the difference between the network parameter a_0 and the pore diameter, Dp [55–56].

The BET surface area for the SBA-15 samples also increased in subsequent generations, starting from 550 $m^2.g^{-1}$ for the first generation and reaching 600 $m^2.g^{-1}$ by the last generation of the synthesis. The wall thicknesses for the SBA-15 samples were around 6 nm for the first and second generation, with a small drop in the third generation to 5.51 nm. However, all of these values are in accordance with that found in the literature [5] and indicate a greater thermal and hydrothermal stability than that to MCM-41. All BET surface area values for the MCM-41 and SBA-15 samples are in line with those found in the literature [57–60].

The thermogravimetric analysis of the synthesized MCM-41 (MCM-41 1G, MCM-41 2G, and MCM-41 3G) and SBA-15 (SBA-15 1G, SBA-15 2G, and SBA-15 3G) samples are shown in Fig. 6 (a) and (b), respectively.

From the thermogravimetric curves of the samples of the synthesized MCM-41 represented in Fig. 6 (a), three mass loss events can be observed for all samples. The first event below 150°C related to the desorption of physiosorbed water in the pores of the MCM-41 that corresponds to 4 % of loss of mass, the second in the range of 150–320°C attributed to the decomposition of the template (CTAB) where the greatest mass loss of 31 % and the third between 400–550°C due to the residual removal of CTAB from the secondary condensation process of the silanol groups corresponding to 13 % of the total loss [37].

The thermogravimetric curves of the synthesized SBA-15 samples (Fig. 6 (b)) indicate two mass loss events, the first below 100°C with 5 % loss relative to the adsorption of physically adsorbed water and the

second between 300 and 400°C with 45 % of loss corresponding to the decomposition of the surfactant (Pluronic P123) occluded in the pores of the molecular sieve [61–62]. These events can be observed in all samples SBA-15 and it is noticeable. Also a sharp peak of DTG between 300 and 400°C regarding the elimination of surfactant P123 [63–64].

4 Conclusions

The synthesis process using the mother liquor was able to produce the structures of the mesoporous sieves MCM-41 and SBA-15 in all three generations, as determined by the X-ray diffractograms (XRD), which showed characteristic peaks in the structure of these materials. The calcination process carried out on the molecular sieves to remove the template was verified by the IR obtained, in which the presence of organic functional groups was not found in the structure of any the calcined samples. All the characterizations carried out on the MCM-41 and SBA-15 mesoporous molecular sieves from the three consecutive syntheses obtained from the mother liquor showed very similar chemical, physical, and morphological properties. The samples obtained from three subsequent cycles exhibited remarkably high BET specific surface areas (above 500 $m^2 \cdot g^{-1}$) and high pore volumes (above 0.60 $cm^3 \cdot g^{-1}$) while maintaining their well-ordered hexagonal mesostructures.

This method of synthesis demonstrated significant relevance in the reduction of effluents generated from the neutralization of the conventional synthesis of these mesoporous materials. Using a simple multi-cycle method, MCM-41 and SBA-15 nanoporous material can therefore be synthesized in a more eco-friendly and economical way.

Declarations

Acknowledgements

The authors are grateful financial support provided by Coordenação de Aperfeiçoamento de Pessoal de NívelSuperior (CAPES).

Funding statement

This study was funded Coordenação de Aperfeiçoamento de Pessoal de Nível Superior (CAPES).

Conflict of Interest

The authors declare that they have no conflict of interest.

Author contributions

Conceptualization, Thianne S. B. Barbosa and Thiago R. B. Barros; methodology, Thianne S. B. Barbosa and Thiago R. B. Barros; writing - original draft preparation, Thianne S. B. Barbosa; writing - review and

editing, Tellys L. A. Barbosa and Meiry G. F. Rodrigues. All authors have read and agreed to the published version of the manuscript.

Availability of data and material

Not applicable.

Compliance with ethical standards

Not applicable.

Consent to participate

Not applicable.

Consent for Publication

Not applicable.

Authors' information (optional)

Thianne Silva Batista Barbosa ORCID: 0000-0002-1828-8546

Thiago Rodrigo Barbosa Barros ORCID: 0000-0002-0857-2017

Tellys Lins Almeida Barbosa ORCID: 0000-0002-3733-4333

Meiry Gláucia Freire Rodrigues ORCID: 0000-0003-2258-4230

References

[1] Wang Y, Li L, Liu Y, Ren X.; Liang J (2016) Antibacterial mesoporous molecular sieves modified with polymeric N-halamine. Mater Sci Eng C 69:1075-1080. doi:10.1016/j.msec.2016.08.017

[2] Jaroszewska K, Masalska A, Czycz D, Grzechowiak J (2017) Activity of shaped Pt/AlSBA-15 catalysts in n-hexadecane hydroisomerization. Fuel Pro Tech 167:1-10. doi:10.1016/j.fuproc.2017.06.012

[3] Costa JAS, Jesus RA, Santos DO, Mano JF, Romão LPC, Paranhos CM (2020) Recent progresses in the adsorption of organic, inorganic, and gas compounds by MCM-41-based mesoporous materials. Micro Meso Mater 291:109698. doi:org/10.1016/j.micromeso.2019.109698

[4] Wan Y, Zhao D (2009) Ordered mesopouros material. In: Jong KP (eds) Synthesis of solid catalyst. Weinhein, Wiley, pp 423

[5] Meynen V, Coll P, Vansat EF (2009) Verified syntheses of mesoporous materials. Micro Meso Mater 125:170–223. doi:10.1016/j.micromeso.2009.03.046

[6] Ying JY, Mehnert CP, Wong MS (1999) Synthesis and applications of Supramolecular-Templated Mesoporous Materials. Angew C Inter Ed 38:56-77. doi:10.1002/(sici)1521-3773(19990115)38:1/2<56::aid-anie56>3.0.co;2-e

[7] Beck JS, Artuli JC, Roth WJ, Leonowicz ME, Kresge CT et al (1992) A new family of mesoporous molecular sieves prepared with liquid crystal templates. J Amer Chem Soc 114:10834-10843. doi:10.1021/ja00053a020

[8] Cai Q, Lin WY, Xiao FS, Pang WQ, Chen XH, Zou BS (1999) The preparation of highly ordered MCM-41 with extremely low surfactant concentration. Micro Meso Mater 32:1-15. doi:10.1016/s1387-1811(99)00082-7

[9] Zhao E, Huo Q, Feng J, Chmelka BF, Stucky GD (1998) Nonionic Triblock and Star Diblock Copolymer and Oligomeric Surfactant Syntheses of Highly Ordered, Hydrothermally Stable, Mesoporous Silica Structures. J Amer Chem Soc 120:6024-6036. doi.org/10.1021/ja974025i

[10] Liu J, Yu J (2016) Toward Greener and Designed Synthesis of Zeolite Materials. In: Zeolites and Zeolite-like Materials. doi:10.1016/b978-0-444-63506-8.00001-x

[11] Duan F, Li J, Chen P, Yu J, Xu R (2009) A low-cost route to the syntheses of microporous cobalt-substituted aluminophosphates by using the waste mother-liquor. Micro Meso Mater 126:26-31. doi:10.1016/j.micromeso.2009.05.015

[12] Liu Z, Li H, Zhang T, Wang Y et al (2020) Mother liquor induced preparation of SAPO-34 zeolite for MTO reaction. Cataly Tod 358:109-115. doi:10.1016/j.cattod.2020.03.034

[13] Ghrear TMA, Ng EP, Vaulot C, Daou TJ, Ling TC, Tan SH, Ooi BS, Mintova S (2020) Recyclable synthesis of Cs-ABW zeolite nanocrystals from non-reacted mother liquors with excellent catalytic henry reaction performance. J Environ Chem Eng 8:103579. doi.org/10.1016/j.jece.2019.103579

[14] Yang J, Huang Y-X, Pan Y, Mi J-X (2020) Green synthesis and characterization of zeolite silicalite-1 from recycled mother liquor. Micro Meso Mater 303:110247. doi:10.1016/j.micromeso.2020.110247

[15] Sahin F, Topuz B, Kalipçilar H (2018) Synthesis of ZIF-7, ZIF-8, ZIF-67 and ZIF-L from recycled mother liquors. Micro Meso Mater 261:259-267. doi:10.1016/j.micromeso.2017.11.020

[16] Zhong J, Han J, Wei Y, Tian P, Guo X, Song C, Liu Z (2017) Recent advances of the nano-hierarchical SAPO-34 in the methanol-to-olefin (MTO) reaction and other applications. Cat Sci Tech 7:4905–4923. doi:10.1039/c7cy01466j

[17] Xi D, Sun Q, Chen X, Wang N, Yu J (2015) The recyclable synthesis of hierarchical zeolite SAPO-34 with excellent MTO catalytic performance. Chem Comm 51(60):11987–11989. doi:10.1039/c5cc03904e

[18] Ng E-P, Goh J-Y, Ling TC, Mukti RR (2013) Eco-friendly synthesis for MCM-41 nanoporous materials using the non-reacted reagents in mother liquor. Nan Res Let 8:120. doi:10.1186/1556-276x-8-120

[19] Chen TL, Kim H, Pan SY, Tseng PC, Lin YP, Chiang PC (2020) Implementation of green chemistry principles in circular economy system towards sustainable development goals: Challenges and perspectives. Sci T Environ 716:136998. doi:10.1016/j.scitotenv.2020.136998

[20] Anastas P, Eghbali N (2010) Green Chemistry: Principles and Practice. Chem Soc Reviews 39:301-312. doi:10.1039/b918763b

[21] Paula GM, Paula LNR, Rodrigues MGF (2020) Production of MCM-41 and SBA-15 hybrid silicas from industrial waste. Silicon. doi: 10.1007/s12633-020-00831-5

[22] Paula LNR, Paula GM, Rodrigues MGF (2020) Adsorption of reactive blue BF-5G dye on MCM-41 synthesized from Chocolate clay. Cerâmica 66:269-276. doi.org/10.1590/0366-69132020663792862

[23] Rodrigues JJ, Fernandes FAN, Rodrigues MGF (2020) The use of cobalt/ruthenium catalyst supported in SBA-15 in the promotion of Fischer-Tropsch synthesis. Braz J Petrol Gas 14:007-021. doi.org/10.5419/bjpg2020-0002

[24] Jovelino JR, Rodrigues JJ, Rodrigues MGF (2018) SBA-15 molecular sieve: synthesis, characterization, and application in oil/water separation. Braz J Petrol Gas 12:219-227. doi.org/10.5419/bjpg2018-0020

[25] Rodrigues JJ, Fernandes FAN, Rodrigues MGF (2018) Co/Ru/SBA-15 catalysts synthesized with rice husk ashes as silica source applied in the Fischer-Tropsch synthesis. Braz J Petrol Gas 12:169-179. doi.org/10.5419/bjpg2018-0016

[26] Silva MM, Patrício ACL, Sousa AKF, Rodrigues MGF, Silva MLP (2015) Synthesis and characterization of MCM-41 By XRD, adsorption capacity and Foster Swelling tests. Mater Sci For 805:657–661. doi:10.4028/www.scientific.net/MSF.805.657

[27] Nogueira AC, Rodrigues JJ, Lima LA, Rodrigues MGF (2015) Preparation and characterization of catalysts Fe/SBA-15 for Fischer-Tropsch synthesis. Mater Sci For 805:678–683. doi:10.4028/www.scientific.net/MSF.805.678

[28] Rodrigues JJ, Nogueira AC, Rodrigues MGF (2015) Rapid synthesis of mesoporous molecular sieve SBA-15 by different techniques with microwave assistance. Mater Sci For 805:684-689. doi:10.4028/www.scientific.net/MSF.805.684

[29] Lima LA, Menezes VMR, Rodrigues MGF (2014) Use residue of bagasse sugar canein synthesis of molecular sieve MCM-41. Mater Sci For 798-799:95–99. doi:10.4028/www.scientific.net/MSF.798-799.95

[30] Paula GM, Lima LA, Rodrigues MGF (2014) SBA-15 Molecular sieve using clay as silicon sources. Mater Sci For 798-799:116-120. doi:10.4028/www.scientific.net/MSF.798-799.116

[31] Rodrigues JJ, Lima LA, Paula GM, Rodrigues MGF (2014) Synthesis and characterization of molecular sieve SBA-15 and catalysts Co/SBA-15 and Ru/Co/SBA-15. Mater Sci For 798:100–105. doi:10.4028/www.scientific.net/MSF.798-799.100

[32] Rodrigues JJ, Fernandes FAN, Rodrigues MGF (2013) Study of Co/SBA-15 catalysts prepared by microwave and conventional heating methods and application in Fischer-Tropsch synthesis. App Cat A Gene 468:32–37. doi.org/10.1016/j.apcata.2013.08.035

[33] Rodrigues JJ, Pecchi G, Fernandes FAN, Rodrigues MGF (2012) Ruthenium Promotion of Co/SBA-15 catalysts for Fischer–Tropsch synthesis in slurry-phase reactors. J Nat Gas Chem 21:722-728. doi:10.1016/S1003-9953(11)60425-8

[34] Rodrigues JJ, Lima LA, Lima WS, Rodrigues MGF, Fernandes FAN (2011) Fischer-Tropsch synthesis in Slurry-Phase reactores using Co/SBA-15 catalysts. Braz J Petrol Gas 5:149–157. doi.org/10.5419/bjpg2011-0015

[35] Sousa BV, Rodrigues MGF, Cano LA, Cagnoli MV, Bengoa JF, Marchetti SG, Pecchi G (2011) Study of the effect of cobalt content in obtaining olefins and paraffins using the FischerTropsch reaction. Catal Tod 172:152-157. doi:10.1016/j.cattod.2011.02.035

[36] Lu D, Xu S, Qiu W, Sun Y, Liu X, Yang J, Ma J (2020) Adsorption and desorption behaviors of antibiotic ciprofloxacin on functionalized spherical MCM-41 for water treatment. J Clea Prod 264:121644. doi:10.1016/j.jclepro.2020.121644

[37] Bezerra DM, Zapelini I W, Franke KN, Ribeiro ME, Cardoso D (2019) Investigation of the structural order and stability of mesoporous silicas under a humid atmosphere. Mater Charact 154:103-115. doi:10.1016/j.matchar.2019.05.032

[38] Adrover ME, Pedernera M, Bonne M, Lebeau B, Bucalá V, Gallo L (2020) Synthesis and characterization of mesoporous SBA-15 and SBA-16 as carriers to improve albendazole dissolution rate. Sau Pharma J 28:15-24. doi:10.1016/j.jsps.2019.11.002

[39] Marinho JC, Barbosa TLA, Rodrigues MGF (2018) Preparation of molecular sieve Al-SBA-15 with two ratios Si/Al catalyst for use in the transesterification reaction of soybean oil. Mater Sci For 912:39-43. doi:10.4028/www.scientific.net/msf.912.39

[40] Wijaya DP, Trisunaryanti W, Dewi TK, Marsuki MF (2018) Synthesis and characterization Of K_2O/MCM-41 (Mobil Composition of Matter No. 41) from lapindo mud by sonochemical method for transesterification catalyst of used cooking oil. Orie J Chem 34(4):1847–1853. doi:10.13005/ojc/3404019

[41] Cotea VV, Luchian CE, Bilba N, Niculaua M (2012) Mesoporous silica SBA-15. a new adsorbent for bioactive polyphenols from red wine. Analy Chim Acta 732:180-185. doi:10.1016/j.aca.2011.10.019

[42] Koh CA, Nooney R, Tahir S (1997) Characterization and catalytic properties of MCM-41 and Pd/MCM-41 materials. Cataly Let 47:199-205. doi.org/10.1023/A:1019025609426

[43] Zholobenko V, Garforth A, Dwyer J (1997) TGA-DTA study on calcination of zeolitic catalysts. Thermo Acta 294:39-44. doi:10.1016/s0040-6031(96)03140-1

[44] Holmes SM, Zholobenko VL, Thursfield A, Plaisted RJ, Cundy CS, Dwyer J (1998) In situ FTIR study of the formation of MCM-41. J Chem Soc Faraday Trans 94:2025–2032. doi:10.1039/a801898g

[45] Marinescu G, Culita DC, Romanitan C, Somacescu S et al (2020) Novel hybrid materials based on heteroleptic Ru(III) complexes immobilized on SBA-15 mesoporous silica as highly potent antimicrobial and cytotoxic agents. Appl Surf Sci 520: 146379. doi.org/10.1016/j.apsusc.2020.146379

[46] Wang X, Chan JCC, Tseng YH, Cheng S (2006) Synthesis, characterization and catalytic activity of ordered SBA-15 materials containing high loading of diamine functional groups. Micro Meso Mater 78:58-65. doi.org/10.1016/j.micromeso.2006.05.003

[47] Siverstein RW, Bassler GC (1962) Spectrometric Identification of Organic Compounds. J Chem Educ 39:546-553. doi.org/10.1021/ed039p546

[48] Stuart BH (2004) Infrared Spectroscopy: Fundamentals and Applications. Hoboken: John Wiley & Sons, Australia

[49] Kresge CT, Leonowicz ME, Roth WJ, Vartuli JC, Beck JS (1992) Ordered mesoporous molecular sieves synthesized bay a liquid-crystal template mechanism. Nature 359:710 – 712. doi:10.1038/359710a0

[50] Grün M, Unger KK, Matsumoto A, Tsutsumi K (1999) Novel pathways for the preparation of mesoporous MCM-41 materials control of porosity and morphology. Micro Meso Mater 27:207-2016. doi:10.1016/s1387-1811(98)00255-8

[51] Ferrer DM, Banda JAM, Rodrigo RS, García UP, Gómez JYV, Vicente PDA (2018) Synthesis of Micro/nanostructured Carbon from Refined Sugar and its Electrochemical Performance. Inter J Electrochem Sci 13:708-718. doi: 10.20964/2018.01.65

[52] Katiyar A, Yadav S, Smirniotis PG, Pinto NG (2006) Synthesis of ordered large pore SBA-15 spherical particles for adsorption of biomolecules. J Chromatography 1122:13–20. doi:10.1016/j.chroma.2006.04.055

[53] Chao MC, Lin HP, Sheu HS, Mou CY (2002) A study of morphology of mesoporous silica SBA- 15. Stud Surf Sci Catal 141:387-394.

[54] IUPAC Recommendations (1985) Pure Appl Chem 57:603-619.

[55] Lin YW, Cheng TW, Lo KW, Chen CY, Lin KL (2020) Synthesis and characterization of a mesoporous Al-MCM-41 Molecular Sieve Material and its Moisture Regulation Performance in Water Molecule Adsorption/Desorption. Micro Meso Mater 310:110643. doi.org/10.1016/j.micromeso.2020.110643

[56] Schwank AJ, Melo DMA, Silva AO, Pergher SBC (2013) Use of rice husk ash as only source of silica in the formation of mesoporous materials. Cerâmica 59:181-185. doi:10.1590/s0366-69132013000100022

[57] Zhang Y, Gao F, Wan H, Wu C, et al. (2008) Synthesis. characterization of bimetallic Ce–Fe-SBA-15 and its catalytic performance in the phenol hydroxylation. Micro Meso Mater 113:393-401. https://doi.org/10.1016/j.micromeso.2007.11.039

[58] Mirji SA, Halligudi SB, Sawant DP, Patil KR., et al. (2006) Adsorption of toluene on Si(100)/SiO_2 substrate and mesoporous SBA-15. Colloids Surf A 272:220-226.

https://doi.org/10.1016/j.colsurfa.2005.07.019

[59] Bérubé F, Kaliaguine S (2008) Calcination and thermal degradation mechanisms of triblock copolymer template in SBA-15 materials. Micro Meso Mater 115:469-479.

https://doi.org/10.1016/j.micromeso.2008.02.028

[60] Yin Y, Wen Z.-H, Liu X-Q, Yuan. A-H, Shi L (2017) Functionalization of SBA-15 with CeO_2 nanoparticles for adsorptive desulfurization: Matters of template P123. Adsorption Science & Technology. DOI: 10.1177/0263617417734767

[61] Janus R, Wadrzyk M, Lewandowski M, Natkanski P, Latka P, Kustrowaki P (2020) Understanding porous structure of SBA-15 upon pseudomorphic transformation into MCM-41: Non-direct investigation by carbon replication. J Indus Engine Chem 92: 131-144. doi:10.1016/j.jiec.2020.08.032

[62] Janus R, Wadrzyk M, Natkanski P, Cool P, Kustrowaki P (2018) Dynamic adsorption-desorption of methyl ethyl ketone on MCM-41 and SBA-15 decorated with thermally activated polymers. J Indus Engine Chem doi.org/10.1016/j.jiec.2018.12.004

[63] Deng X, Chen K, Tuysuz H (2017) Protocol for the Nanocasting Method: Preparation of Ordered Mesoporous Metal Oxides. Chem Mater 29:40-52 doi:10.1021/acs.chemmater.6b02645

[64] Serrano DP, Calleja G, Botas JA. Gutierrez FJ (2004) Adsorption and hydrophobic properties of mesostructured MCM-41 and SBA-15 materials for volatile organic compound removal. Indus Engine Chem Resear 43:7010-7018. doi:10.1021/ie040108d

Figures

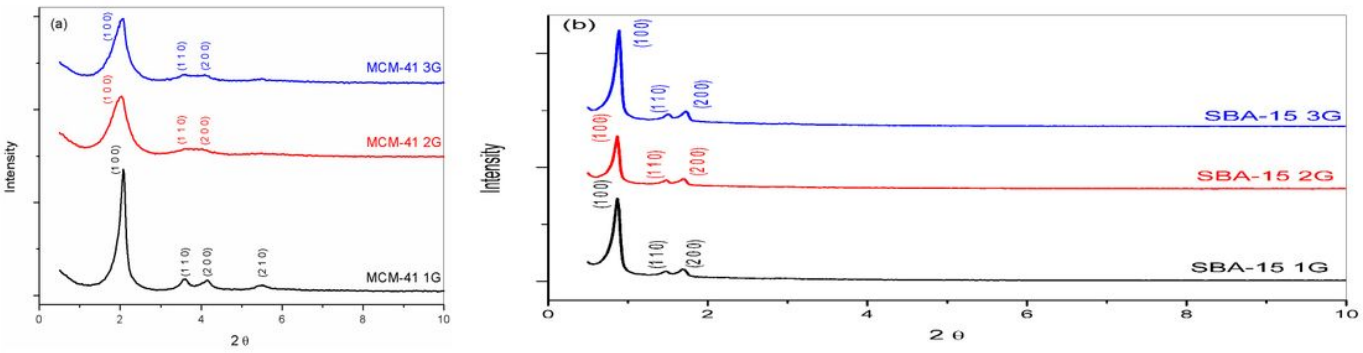

Figure 1

Fig. 1 (a) shows the diffractograms of the samples of MCM-41 synthesized initially (MCM-41 1G) and from the following generations MCM-41 2G and MCM-41 3G. The diffractograms of the synthesized SBA-15 samples (SBA-15 1G, SBA-15 2G and SBA-15 3G) are shown in Fig. 1 (b).

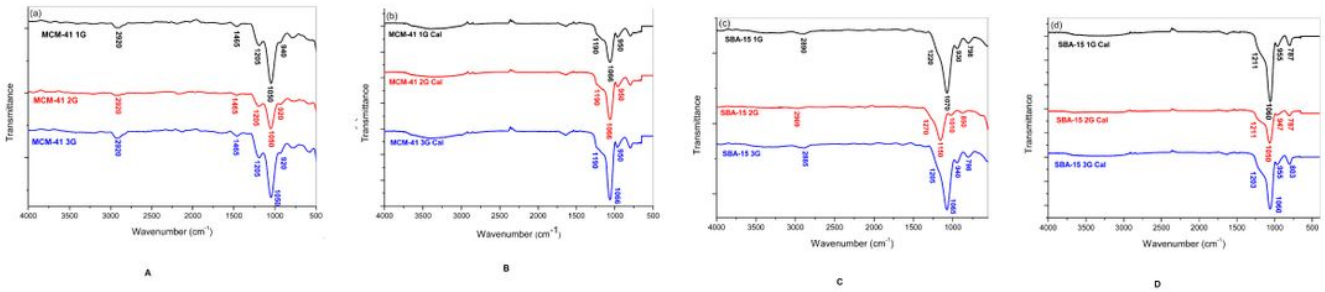

Figure 2

The spectra of the synthesized (MCM-41 1G, MCM-41 2G, and MCM-41 3G) and calcined (MCM-41 1G Cal, MCM-41 2G Cal, and MCM-41 3G Cal) samples are shown in Fig. 2 (a) and (b), respectively. The spectra of the synthesized (SBA-15 1G, SBA-15 2G, and SBA-15 3G) and calcined (SBA-15 1G Cal, SBA-15 2G Cal, and SBA-15 3G Cal) samples are shown in the Fig. 2 (c) and (d), respectively.

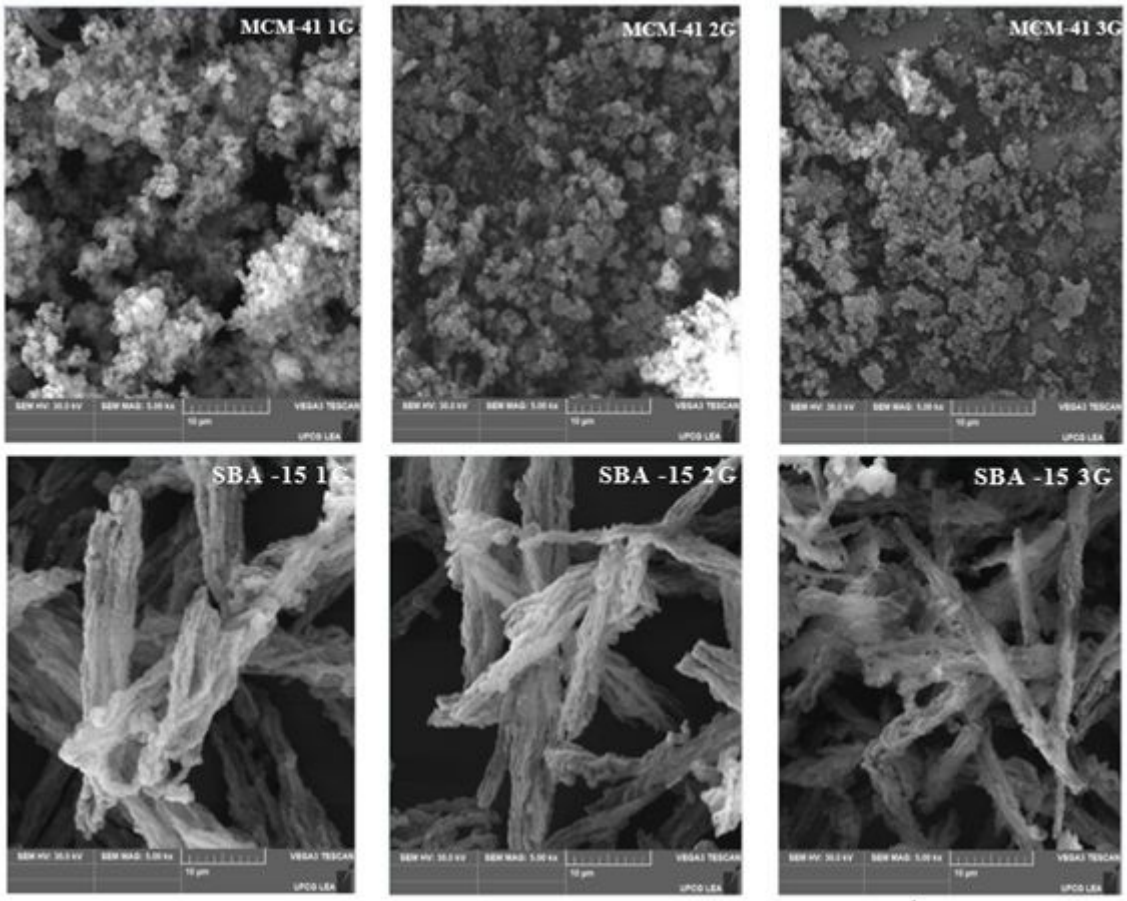

Figure 3

Fig. 3 shows the images obtained through SEM for the synthesized MCM-41 samples (MCM-41 1G, MCM-41 2G, and MCM-41 3G) and synthesized SBA-15 samples (SBA-15 1G, SBA-15 2G, and SBA-15 3G).

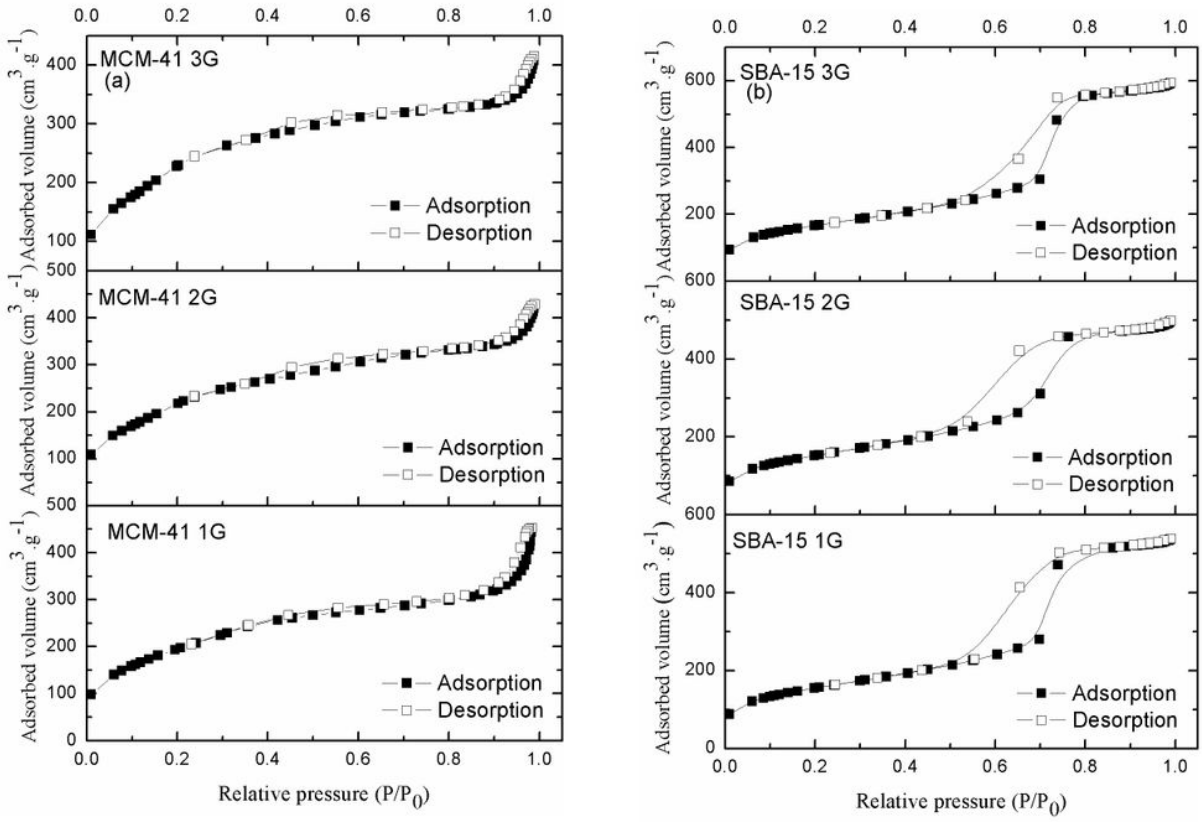

Figure 4

Fig. 4 shows the adsorption and desorption isotherms of the MCM-41 and SBA-15 samples, obtained through the BET method. All samples exhibited type IV isotherms, according to the IUPAC classification, with different hysteresis loops shown for the MCM-41 and SBA-15 samples [54].

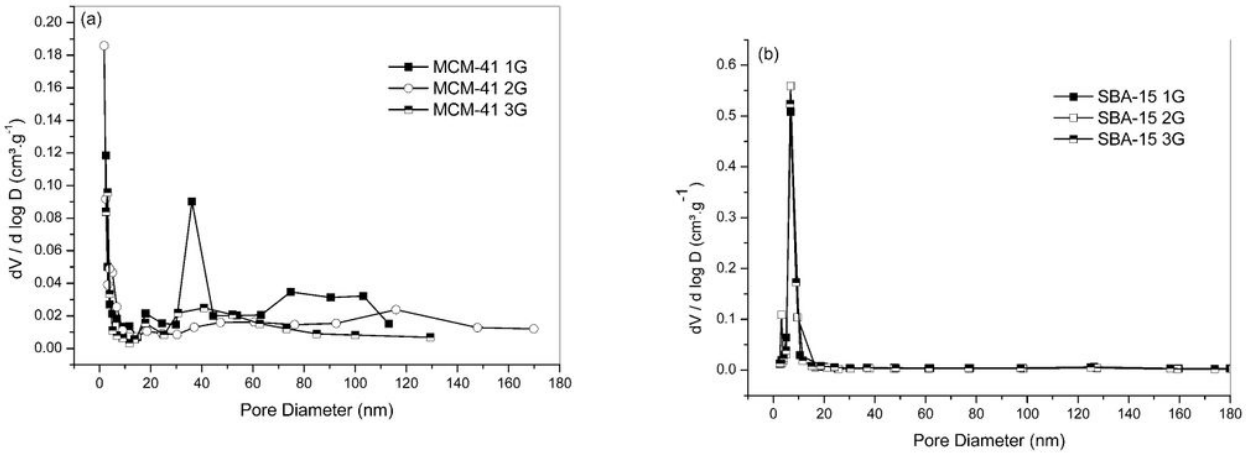

Figure 5

The graphs of the pore distributions of the MCM-41 and SBA-15 samples, as obtained through the BJH method, are shown in Fig. 5 (a) and (b), respectively.

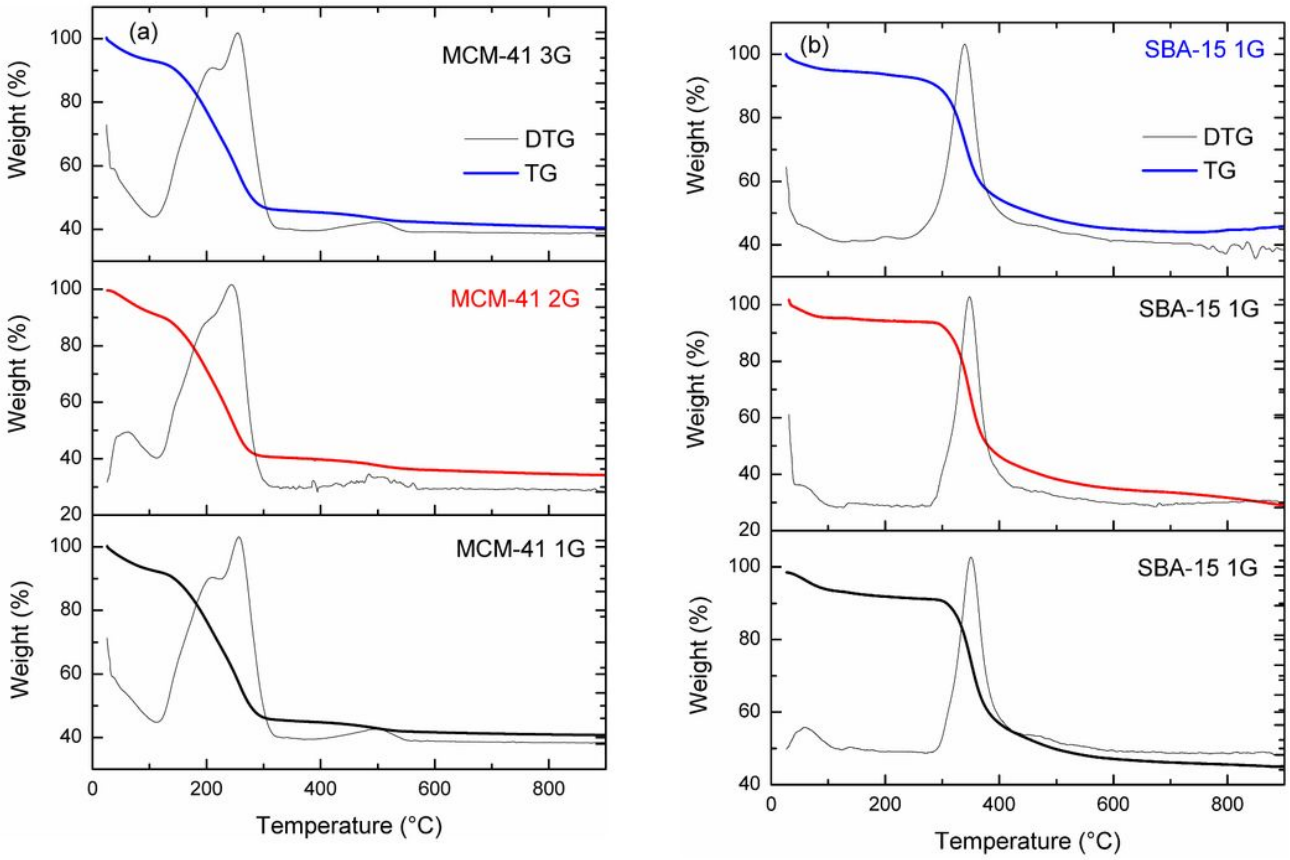

Figure 6

The thermogravimetric analysis of the synthesized MCM-41 (MCM-41 1G, MCM-41 2G, and MCM-41 3G) and SBA-15 (SBA-15 1G, SBA-15 2G, and SBA-15 3G) samples are shown in Fig. 6 (a) and (b), respectively.